Macromolecular Chemistry and Physic
www.mcp-journal.d

Selective Recognition of Fe(III) in Aqueous Environment over Covalently-Bonded Tb-Complex-Containing Fluorescent Porous Copolymer Microspheres

Chunyan Zhang, Jianxin Luo, Wenjun Li, Lijuan Ou, Guipeng Yu,* and Chunyue Pan**

An environment-friendly synthesis of a covalently bonded terbium(Tb)-complex-containing monodispersed fluorescent porous copolymer microspheres, and their highly selective detection of Fe^{3+} are described. The as-made copolymer microspheres exhibit intense green fluorescence originating from Tb ions and high photostability in water. Encouragingly, the fluorescence of the copolymer microspheres can be selectively quenched by trace Fe^{3+} due to the interaction between Fe^{3+} and the ligands, which disturbs the coordination structure of Tb-complexes and inhibits the energy transfer from ligands to Tb ions. The intense fluorescence intensity, high fluorescence stability, together with the nanoscale and porous nature of the copolymer microsphere endows them with wide detection range (0–1500 μM) and low detection limit (2.1 μM) for selective recognition of Fe^{3+} in aqueous environment. This study paves a new pathway for the function of porous copolymer microspheres being used as targeting for biological detection and environmental issues.

1. Introduction

Detection of specific metal ions has attracted considerable attention due to their essential application in life science and environmental science in recent years.[1,2] Particularly, iron is indispensable for most organisms, and both its deficiency and overload can cause various disorders. Therefore, the development of reliable sensing methods for iron ions is very important for human health and environment protection.[3–6] Due to the advantages of simple, rapid, and non-destructive characteristics, many fluorescence sensors for iron-selective assay have been reported in last decades.[6–11] However, most of the reported Fe^{3+} sensors have some shortcoming, such as poor fluorescence stability, tedious preparation procedures requiring toxic, or expensive raw materials. Therefore, the development of water-soluble, photostable, and improved selective and sensitivity Fe^{3+} sensors using simple, cost-effective, and environment-friendly preparation procedures remains highly desirable.

Owing to unique photophysics properties such as wide excitation bands, sharp emission peaks, long emission lifetimes, and large Stokes shift, lanthanide complexes (Ln-complexes) have attracted great interests in the field of Fe^{3+} sensors.[12–15] Unfortunately, most of the reported Ln-complexes are unstable and sensitive to outside species due to the complexes can be easily disturbed by competing ligands, metal ions, acidic, or alkaline substances. A prevalent solution is incorporating Ln-complexes into organic framework, polymers, inorganic, or hybrid matrices.[12,16–33] Polymer microspheres are cost-effective, easily available, and have convenient functionalization, which can provide hydrophobic environment to protect the Ln-complexes from being disturbed by outside species. In addition, the introduction of functional groups, such as carboxyl acid groups and amino groups, on the surface of polymer microspheres can overcome its disadvantage of poor water-solubility, and widen its practical application in aqueous medium. Therefore, it is a promising way to use functionalized polymer microspheres as substrates for Ln-complexes. In fact, lanthanide ions or their complexes have been incorporated or doped into the interior or tagged on the surface of the microspheres by non-covalent[27,28] or covalent binding process.[29,30] The covalently-bonded strategy can avoid the leakage of Ln-complexes, and ensure the photostability of the corresponding fluorescent polymer microspheres. Several polymerization approaches (such as, emulsion, dispersion, and suspension polymerization) are available to prepare fluorescent polymer microspheres. In particular, soap-free emulsion polymerization without surfactants can produce clean monodisperse microspheres, which have been used to prepare Eu complex–based fluorescent microspheres.[17]

To the best of our knowledge, there have been few reports on the emulsion copolymerization of terbium(Tb)-complex monomers with other vinyl monomer until now. Particularly, the introduction of functional monomers such as Tb-complex monomers in the emulsion copolymerization usually leads to

Dr. C. Y. Zhang, Prof. G. P. Yu, Prof. C. Y. Pan
College of Chemistry and Chemical Engineering
Hunan Provincial Key Laboratory of Efficient and Clean Utilization of Manganese Resources
Central South University
Changsha 410083, Hunan, China
E-mail: gilbertyu@csu.edu.cn; panchunyue@csu.edu.cn
Dr. C. Y. Zhang, Dr. J. X. Luo, Dr. W. J. Li, Dr. L. J. Ou
Department of Materials and Chemical Engineering
Hunan Institute of Technology
Hengyang 421002, Hunan, China
E-mail: luojianxin392@163.com
The ORCID identification number(s) for the author(s) of this article can be found under https://doi.org/10.1002/macp.201800403.

DOI: 10.1002/macp.201800403

the loss of control over particle size and size distribution.[18] In this work, covalently bonded Tb-complex-containing fluorescent copolymer microspheres were prepared by soap-free emulsion polymerization of styrene (St) with Tb-complex monomer. Meanwhile, methacrylic acid (MAA) and divinylbenzene (DVB) were used as the water-soluble monomer and cross-linked monomer, respectively. The carboxyl can ensure preferably water-dispersibility, and Tb-complex monomer may endow the copolymer microspheres with intense fluorescence and task-specific sensing properties. The obtained Tb-complex-containing copolymer microspheres may find promising applications in optical devices or fluorescence sensors.

2. Experimental Section

2.1. Materials

Styrene (St), acrylic acid (AA), and methacrylic acid (MAA) were purified by distillation under reduced pressure and stored at 5 °C. Divinylbenzene (DVB), 1,10-phenanthroline (Phen), and terbium oxide (Tb_4O_7) were purchased from Aladdin Industrial Corporation and used as received. Hydrochloric acid, ethanol and ammonia were purchased from Guangzhou Chemical Reagent (in China). Potassium peroxydisulfate (KPS) was purified by recrystallization in distilled water and then dried under vacuum. Tb-complex monomer ($Tb(AA)_3Phen$) was synthesized according to the reported procedures with slightly modification,[17] Supporting Information. Distilled water was used throughout the experiments.

2.2. Preparation of Tb-Complex-Containing Copolymer Microspheres

Tb-complex-containing copolymer microspheres were prepared by soap-free emulsion polymerization. Briefly, 80 mL distilled water was stirred for 30 min at 70 °C in 250 mL jacketed reaction vessel fitted with nitrogen flow, overhead stirrer, and condenser. A mixture of 8 g St, 1 g MAA, and $Tb(AA)_3Phen$ was added to the reaction vessel and stirred for 15 min, then a dissolved solution (10 mL) of 0.1 g KPS was added and stirring was continued at 70 °C. After 2 h, 1 g DVB was added to the mixture. Polymerization continued for 24 h at an appropriate stirring speed. Reaction mixture was cooled to room temperature and was washed multiple times via centrifugation and resuspension in distilled water. The products were dried at 60 °C in vacuum for one day and labeled as n-PSTb-0 – n-PSTb-5.

2.3. Measurements

Monomer conversion (Conv.) was determined by gravimetric analysis. ^{13}C CP/MAS NMR spectra were recorded on Bruker Advance III HD 400 NMR spectrometer at an MAS rate of 5.0 kHz using zirconia rotors 4 mm in diameter. FT-IR spectra were recorded in transmission on a Spectrum One PerkinElmer using KBr pellets. Elemental analyses (C, H, and N) were performed with a Vario EL analyser. Acid–base titration was carried out as described by Liang et al.[19] The morphology of the microspheres were observed by scanning electron microscopy (SEM, JEM-7100F, JEOL) at an accelerating voltage of 5 kV. Transmission electron microscopy (TEM) was carried out on a JEOL JEM-electron microscope operating at 200 kV. The size and zeta-potential of the microspheres were measured by Nano-size and Zeta-potentiometer Analyser (Malvern Zetasizer Nano ZS90, UK). Surface element composition were determined by X-ray photoelectron spectroscopy (ESCALAB 250Xi, Thermo Fisher-VG Scientific, USA). Nitrogen adsorption/desorption isotherms were measured at 77 K by using an Autosorb-iQ (Quantachrome) analyzer. Surface areas were calculated by the Brunauer–Emmett–Teller (BET) method and pore-size distributions were evaluated from the N_2 adsorption isotherms using the Barrett–Joyner–Halenda (BJH) model. The glass transition temperature (T_g) was studied by differential scanning calorimetry (DSC Q20, TA Instrument, USA) at a heating rate of 10 °C min^{-1} under nitrogen atmosphere. Thermogravimetric analysis (TGA) was performed on a TA Q50 at a heating rate of 20 °C min^{-1} under nitrogen atmosphere. UV–vis absorption spectra were determined on a Shimadz spectrophotometer (UV-2700). Photoluminescence (PL) spectra were recorded with a Cary Eclipse F2500 spectrophotometer. Fluorescence lifetimes (τ) were obtained on a FLS920 steady state spectrometer with a pulsed xenon lamp. Fluorescence quantum yield of the copolymer microspheres was determined by using quinine sulfate (dissolved in 0.5 M H_2SO4 with a concentration of 10^{-5}M, assuming ϕ of 0.55) as a standard.[34] Before photophysical properties measurements, the copolymer microspheres were added into water and oscillated for 5 min using ultrasonic waves to ensure uniform dispersion at room temperature. Certain concentration of several metal salts (KCl, $CaCl_2$, $MgCl_2$, $FeCl_3$, $CoCl_2$, $NiCl_2$, $CuCl_2$, $SnCl_2$, $HgCl_2$, $PbCl_2$, $MnSO_4$, $AgNO_3$, $Fe_2(SO_4)_3$, $Fe(NO_3)_3$, and $Fe(Ac)_3$), H_2O_2 and NaClO were added to the dispersion of the copolymer microspheres, the fluorescence spectra of the dispersion were measured. After fluorescence quenching, $NaBH_4$ was added to the dispersion and its fluorescence spectra were recorded.

3. Results and Discussion

3.1. Preparation and Characterization

Novel covalently-bonded Tb-complex-containing copolymer microspheres were prepared through one-step soap-free emulsion polymerization as shown in **Figure 1**. $Tb(AA)_3Phen$ was dispersed in the mixed monomer of St and MAA. Then the monomer mixture was added into water to form oil-in-water droplets in the case of agitation. The stabilization of the droplets depends on the hydrophilic monomers (MAA).[35] Meanwhile, KPS was added and decomposed to generate radical, which initiate MAA to form oligomer. The oligomer radical further initiate oil monomers to form latex particles, which were stabilized by the oligomer and the initiator molecules ($S_2O_8^{2-}$).[33,36] After latex particles were formed, DVB was added to form cross-linked copolymer microspheres. In the above process, water was used as reaction medium, and no emulsifier was added. The preparation process is simple and environment-friendly,

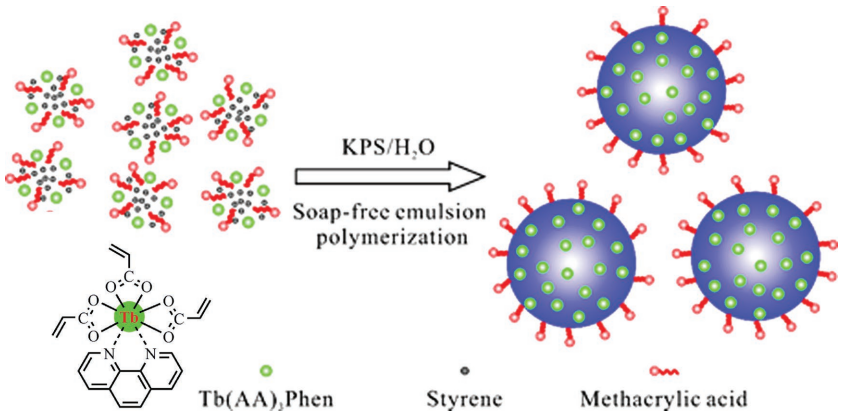

Figure 1. Preparation of Tb-complex-containing copolymer microspheres.

and the prepared microspheres exhibit good water-dispersibility and can be applied to aqueous environment.

Hydrophobic monomers (St and DVB) are concentrated on the interior of the particles, while hydrophilic monomers (MAA and Tb-complex monomer) are easily enriched on the surface (Figure 1). As the amounts of Tb-complex monomer increased, the content of Tb-complex on the surface of the particles increased, while the surface carboxyl content decreased (Table S1, Supporting Information). As a result, the zeta potential (ζ) of the particles decreased and the emulsion gradually became unstable (**Table 1**). Consequently, the precursor particles further aggregated to form large particles. In addition, cross-linkable Tb-complex monomer contained on the surface of the precursor particles is also favorable for cross-linking to form aggregation.[17] Thus it can be seen that the particle size of the copolymer microspheres increased with the increase in the amount of Tb-complex monomer (**Figure 2**a). The average particle size (d) of n-PSTb-0 (without Tb-complex) was about 198 nm and it increased to 496 nm at the Tb-complex contents of about 2.5 wt% (n-PSTb-4). Nevertheless, the particle size distribution index (PDI) of the copolymer microspheres is relatively small, indicating that the copolymer microspheres have a uniform size. However, if the content of Tb-complex is increased to 3.75 wt%, gels were generated, and PDI increased significantly (PDI = 0.489, Table 1). The above results are also illustrated by SEM and TEM images. As illustrated in Figure 2, n-PSTb-4 exhibit a uniform spherical shape with particle size of about 400 nm. It can be also seen from TEM images that the surface of the copolymer microspheres is rough, which further proves the occurrence of particle aggregation as mentioned above.

The ^{13}C CP/MAS NMR spectra of the copolymer microspheres (n-PSTb-0 and n-PSTb-4) are shown in **Figure 3**. The chemical shifts of -CH_3 (f), -CH_2 (b), and -COOH (g) were located at 18, 30, and 178 ppm, respectively. Due to the difference of the substituent (phenyl, and carboxyl), the chemical shifts of –CH were located at (a) 39 ppm, and (e,h) 44 ppm, respectively. The signals around 90–150 ppm can be assigned to aryl. Owing to low Tb-complex content in the copolymer microspheres, the signal peaks of Tb-complex were weak and buried under those of aryl. However, a weak characteristic peak of Phen appeared at (l) 137 ppm can be observed in n-PSTb-4. **Figure 4** depicts the FT-IR spectra of the Tb-complex monomer and the copolymer microspheres (n-PSTb-0 and n-PSTb-4). The peaks that appeared at 1703 and 3470 cm^{-1} were attributed to stretching vibration of carbonyl (C=O) and hydroxyl (O–H) of MAA segments, respectively. The peaks around 1450–1600 cm^{-1} and 700–755 cm^{-1} were attributed to the characteristic signals of C=C and C–H in aryl. The peaks around 3000 cm^{-1} were assigned to the asymmetrical and symmetrical stretching of –CH_3 and –CH_2. Compared to n-PSTb-0, characteristic peaks of Tb-O and Tb-N located around 450 cm^{-1} can be observed in the FT-IR spectrum of n-PSTb-4, which is similar to that of $Tb(AA)_3Phen$. Additionally, only the characteristic peaks of C(1s) and O(1s) appeared in XPS spectra of n-PSTb-0 (Figure S1, Supporting Information), but the signals of N(1s) and Tb(3d) can also be observed in n-PSTb-4. According to the contents of various elements (C, H, and N), the actual contents of Tb-complex ([Tb]) in the copolymer microspheres were calculated roughly and listed in Table 1. Due to steric effect of Tb-complex, the actual content of Tb-complex ([Tb]) was slightly lower than the theoretical content (Tb). Moreover, one can find that high Tb-complex content leads to a large difference between the actual content and the theoretical content. Meanwhile, the inhibition effect of Tb-complex decreased the yield of copolymer microspheres. These results indicate that the Tb-complex has been introduced into the copolymer microspheres successfully.

Table 1. Composition, structure, and properties of the copolymer microspheres.

Microspheres	Tb[a] [wt%]	[Tb][b] [wt%]	Stability	Yield [%]	d[c] [nm]	PDI[c]	ζ[c] [mV]
n-PSTb-0	0	0	Stable	91	198	0.055	–26.9
n-PSTb-1	0.25	0.25	Stable	83	309	0.066	–26.4
n-PSTb-2	0.63	0.62	Stable	78	386	0.062	–25.6
n-PSTb-3	1.25	1.23	Stable	76	465	0.072	–25.7
n-PSTb-4	2.50	2.43	Stable	79	496	0.079	–23.1
n-PSTb-5	3.75	3.68	Unstable	67	564	0.489	–18.3

[a]Theoretical content of Tb-complex monomer calculated according to feed composition based on the amount of styrene; [b]Actual content of Tb-complex monomer calculated according to elemental analyses; [c]Determined by Malvern particle size and Zeta potentiometer.

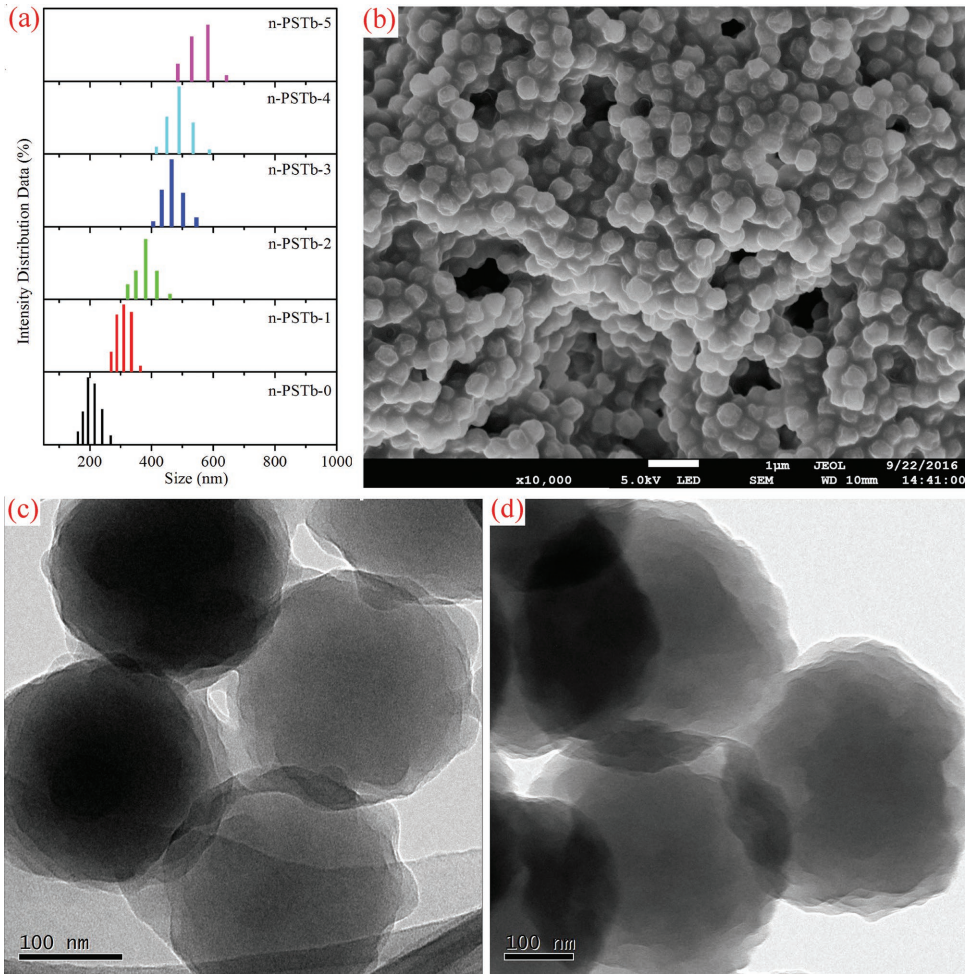

Figure 2. a) Particle size distribution of the copolymer microspheres; b) SEM images of the copolymer microsphere n-PSTb-4; c,d) TEM images of the copolymer microspheres: (c) n-PSTb-0, (d) n-PSTb-4.

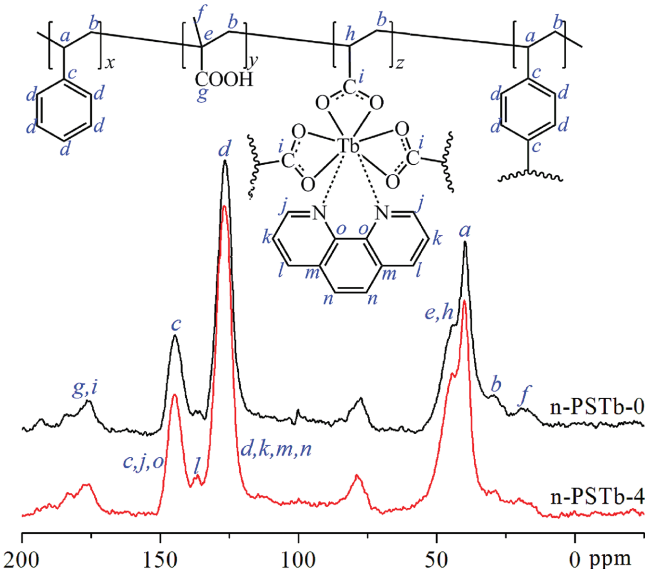

Figure 3. ^{13}C CP/MAS NMR spectra of the copolymer microspheres n-PSTb-0 and n-PSTb-4.

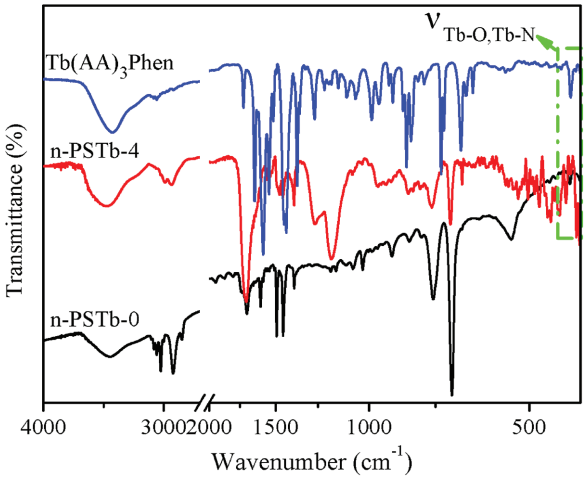

Figure 4. FT-IR spectra of the Tb-complex monomer and the copolymer microspheres (n-PSTb-0 and n-PSTb-4).

3.2. Porosity and Thermal Properties

The porosity of the copolymer microspheres was explored by N_2 sorption experiments at 77 K. The copolymer microspheres display type IV curve with H1-type hysteresis loops at high relative pressure (Figure S2a, Supporting Information). The typical hysteresis of the N_2 adsorption isotherms could be attributed to the steric hindrance of Tb-complex, which reduces the access of N_2. Relative steady rise phase ranges from 0.1 to 0.9 (P/P_0) demonstrate the presence of mesopores.[37,38] In addition, a significant increase in the N_2 uptake at a high relative pressure above 0.9 may arise mainly from interparticulate porosity associated with the meso-/macrostructures of the samples and interparticular void.[39] The pore size distribution curves (Figure S2b, Supporting Information) reveal that the copolymer microspheres mainly displays mesopores with pore size of 2–10 nm, originating from the aggregation of precursor particles, which is consistent with the description of the N_2 adsorption and desorption isotherm. As presented in **Table 2**, with the increase of Tb-complex content at the range from 0 to 2.5 wt%, all the pore parameters increases gradually. Notably, n-PSTb-4 exhibits a high BET surface area and abundant pores, which is beneficial for the contact between Tb-complex and analysts.[12]

DSC curves of the copolymer microspheres with various Tb-complex contents are shown in Figure S3, Supporting Information. All the samples showed a single glass transition temperature (T_g), which increased from 113 to 124 °C with the increase of Tb-complex contents from 0 to 3.75 wt%, respectively, and the results are listed in Table S1, Supporting Information. An increase in the T_g was due to the incorporation of rigid and bulky Tb-complex in the copolymer microspheres. The thermal stability of the copolymer microspheres and the Tb-complex monomer were evaluated by TGA (Figures S4 and S5, Supporting Information). The temperature of 5% weight loss (T_d) of the stable copolymer microspheres is above 293 °C, which is higher than that of Tb-complex monomer (Table S1, Supporting Information). These results indicate that the copolymer microspheres have excellent thermal stability for a wide range of applications such as optoelectronic devices and sensors. The weight percentage of the residue (R_w) of the copolymer microspheres at 800 °C were determined from TGA, and listed in Table S1, Supporting Information. R_w of n-PSTb-0 (without Tb-complex) was close to 0 ($R_w = 0.02$), indicating that polymer segments can be completely decomposed into volatile gases. For Tb-complex-containing copolymer microspheres (n-PSTb-1 – n-PSTb-5), both polymer segments and organic ligands can be completely decomposed into volatile gases at 800 °C, but terbium ions may be converted into terbium oxide, that is residues.[25] With the increase of Tb-complex content, R_w of the copolymer microspheres increases gradually. The results also suggest that the Tb-complex has been introduced into the copolymer microspheres successfully.

3.3. Luminescence Properties

The excitation spectra (Figure S6, Supporting Information) exhibit dominant broad bands in the range of 275–350 nm originating from the characteristic absorption of acrylic acid ligands.[40] As the content of the Tb-complex increases, the intensity of the excitation bands increased gradually. Besides, no apparent sharp excitation peaks of Tb^{3+} can be observed in long wavelength region, suggesting that luminescence sensitization via excitation of ligands is much more efficient than direct excitation of the terbium ion's absorption levels. In comparison with excitation spectra of the Tb-complex monomer (Figure S7, Supporting Information), the excitation bands of the copolymer microspheres broaden and shift to short wavelength (blue-shift), indicating that the coordination environment of Tb-complex has be changed in the copolymer microspheres.[30] The emission spectra in **Figure 5** show characteristic emission peaks of Tb^{3+} at 489, 545, 586, and 620 nm ascribed to the $^5D_4 \rightarrow {}^7F_6$, $^5D_4 \rightarrow {}^7F_5$, $^5D_4 \rightarrow {}^7F_4$, and $^5D_4 \rightarrow {}^7F_3$, respectively.[12] The green emission (545 nm) has maximum intensity, which is consistent with the fluorescence images as shown in the insert of Figure 5. The PL emission intensities (I), as well as luminescent lifetimes (τ) and fluorescence quantum yield (ϕ) of the copolymer microspheres increased with the increasing of Tb-complex content (Table 2), which may be attributed to the increase of both Tb-complex contents and BET surface area.[41] The PL emission intensity of n-PSTb-4 aqueous dispersion is almost not reducing as the time progresses (Figure S8, Supporting Information), implying the perfect fluorescence stability of the copolymer microsphere in aqueous medium. The ability to be compatible with the aqueous environment, as well as the nanoscale and porous nature of the fluorescent copolymer microspheres, makes them highly suitable for generating new fluorescence sensors in biological, medical, and environmental fields.

Table 2. Porous, fluorescence, and sensing properties of the copolymer microspheres.

Microspheres	SA_{BET}[a)] [$m^2\ g^{-1}$]	V_{Tot}[b)] [$cm^3\ g^{-1}$]	$V_{0.1}$[c)] [$cm^3\ g^{-1}$]	$V_{0.1}/V_{Tot}$ [%]	I[d)] [a.u.]	τ [ms]	ϕ [%]	K_{SV}[e)] [$10^4 M^{-1}$]	LOD[f)] [μM]
n-PSCz-0	34	0.36	0.011	3.0	NA	NA	NA	NA	NA
n-PSTb-1	36	0.35	0.011	3.1	77.7	0.49	2.3	0.964	4.2
n-PSTb-2	37	0.37	0.013	3.5	105.9	0.53	3.1	1.018	3.9
n-PSTb-3	39	0.39	0.014	3.6	130.8	0.53	3.4	1.034	3.1
n-PSTb-4	41	0.40	0.021	5.3	207.4	0.54	4.5	1.100	2.1
n-PSTb-5	40	0.39	0.017	4.4	277.5	0.59	5.1	1.087	2.3

[a)]Calculated using adsorption branches over the pressure range 0.01–0.1 bar of N_2 isotherm at 77 K; [b)]Determined from the N_2 isotherm at $P/P_0 = 0.9$ bar; [c)]Determined from the N_2 isotherm at $P/P_0 = 0.1$ bar; [d)]The maximum emission intensity (located at 545 nm) of the water-dispersed copolymer microspheres (1 mg mL^{-1}) at excitation wavelength 300 nm; [e)]Determined by Stern–Volmer equation; [f)]Calculated according to equation: LOD = $3S_d/m$.

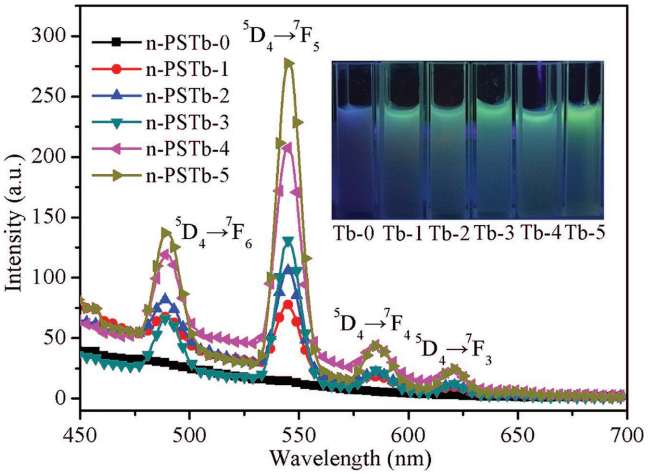

Figure 5. PL emission spectra of the water-dispersed copolymer microspheres (1 mg mL^{-1}) at excitation wavelength 300 nm. Insert of the graph illustrates the fluorescence images of the water-dispersed copolymer microspheres (1 mg mL^{-1}) under UV-light irradiation.

3.4. Sensing Properties

The fluorescence response of n-PSTb-4 toward aqueous solutions of various metal ions are shown in **Figure 6**. Interestingly, only Fe^{3+} exhibits a drastic quenching effect on the luminescence of n-PSTb-4, and the quenching efficiency was nearly 95%. Moreover, other co-existing metal ions have negligible effect on the fluorescence quenching efficiency of n-PSTb-4 with Fe^{3+} (the insert of Figure 6). Additionally, the common anions such as Cl^-, CH_3COO^-, SO_4^{2-}, and NO_3^- also have a negligible effect on the fluorescence quench of n-PSTb-4 with Fe^{3+} (Figure S9, Supporting Information). Therefore, we can conclude that the copolymer microspheres have promising selectivity toward Fe^{3+} detection in aqueous medium.

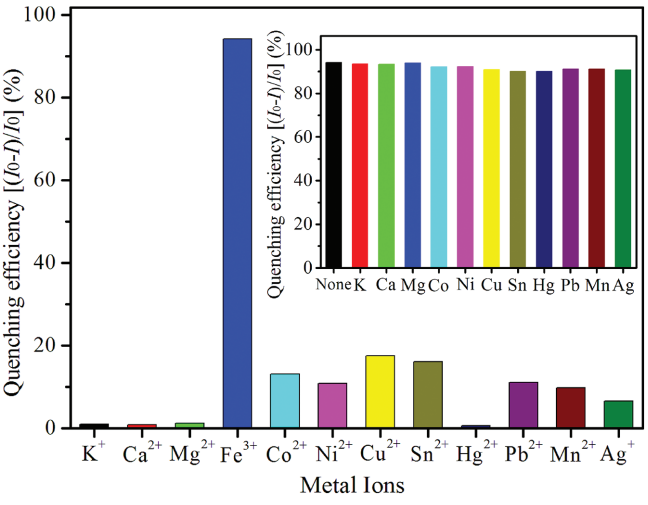

Figure 6. Fluorescence response profiles of n-PSTb-4 in aqueous solutions (1 mg mL^{-1}) upon addition of different metal ions (1500 μM). Insert of the graph illustrates fluorescence response profiles of the copolymer microsphere n-PSTb-4 in aqueous solutions upon addition of the mixture of Fe^{3+} (1500 μM) and other metal ions (1500 μM).

For better understanding the fluorescence response of n-PSTb-4 to Fe^{3+}, the luminescence titration upon the addition of $FeCl_3$ to n-PSTb-4 was further conducted. As demonstrated in **Figure 7**a, the fluorescence intensity of n-PSTb-4 decreased gradually with the increase of Fe^{3+} concentration from 0 to 1500 μM. After adding 1500 μM Fe^{3+}, the green fluorescence of the water-dispersed n-PSTb-4 was almost quenched completely, which is also demonstrated in the fluorescence images as shown in the insert of Figure 7a. However, the shape and position of the emission peaks have not changed, indicating that the tolerance level of Fe^{3+} detection by n-PSTb-4 in aqueous medium can attain to 1500 μM. The results strongly suggest that the copolymer microspheres exhibit a wide detection range for Fe^{3+} from the biological tissue and industrial waste. Quantitatively, the quenching efficiency can be explained using the Stern–Volmer (SV) equation: $I_0/I = 1 + K_{SV}[C]$, where K_{SV} is the quenching constant (M^{-1}), [C] is the Fe^{3+} concentration, I_0

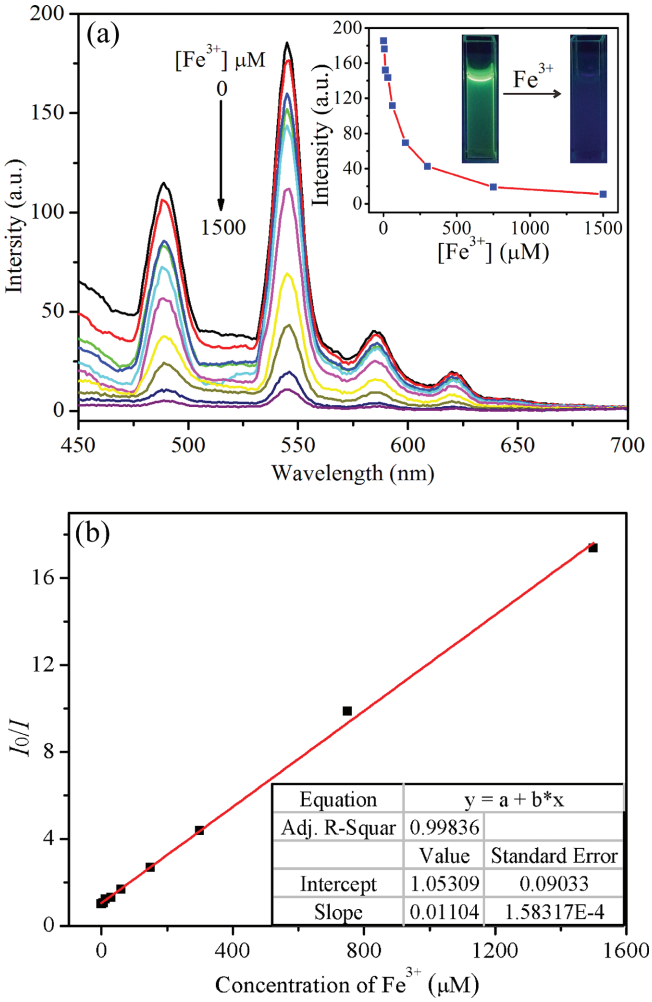

Figure 7. a) Fluorescence response of n-PSTb-4 in aqueous solutions (1 mg mL^{-1}) upon addition of Fe^{3+} under excitation at 300 nm. Insert of the graph illustrates the relationship between the maximum intensity located at 545 nm of n-PSTb-4 and the concentration of Fe^{3+} and the change of fluorescence images (under UV-light irradiation) upon addition of Fe^{3+}. b) Stern–Volmer graph of n-PSTb-4 in aqueous solutions (1 mg mL^{-1}) in the presence of various concentrations of Fe^{3+}.

and I are the luminescence intensities of the water-dispersed copolymer microspheres without and with addition of Fe^{3+}, respectively. As shown in Figure 7b, I_0/I displayed a good linear relationship with the concentration of Fe^{3+} in the range of 0–1500 μM ($R^2 = 0.998$), which can be curve-fitted into $I_0/I = 1.05 + 0.011 \times [Fe^{3+}]$ (μM). The value of K_{SV} was calculated as 1.10×10^4 M^{-1}, which reveals a strong quenching effect on the luminescence of n-PSTb-4. Remarkably, limit of detection (LOD) for Fe^{3+} with n-PSTb-4 in aqueous medium was determined as 2.1 μM, which is comparable to or better than some previously reported fluorescent sensors for Fe^{3+}.[7,8,42] Furthermore, the low LOD meets the permitted valued of Fe^{3+} (5.4 μM) in drinking water by the U.S. Environmental Protection Agency (USEPA) and World Health Organization (WHO).[42]

To further investigate the fluorescence quenching mechanism of the copolymer microsphere with Fe^{3+}, sensing experiments of n-PSTb-4 with other oxidants were conducted. The copolymer microsphere n-PSTb-4 exhibited a weak fluorescence quenching after mixing with H_2O_2 or NaClO in aqueous solutions (Figure S10, Supporting Information). Additionally, the quenched fluorescence of n-PSTb-4 could hardly recover after adding the reducing agent $NaBH_4$ (Figure S11, Supporting Information). The results reveal that the fluorescence quenching of the copolymer microspheres are not due to the oxidation of iron ion.

Compared with other metal ions, Fe^{3+} with a half filled d-electron spherical distribution has the most number of unpaired electrons, which can effectively quench fluorescence.[40,43] Particularly, Fe^{3+} possesses a much higher binding ability to the N and O atoms than other metal ions.[44,45] The possible interaction between iron ions and ligands may disturb the coordination structure of Tb-complexes. In order to verify this result, the absorption spectra of copolymer microsphere n-PSTb-4 before and after addition of Fe^{3+} have been determined. After the addition of Fe^{3+}, the absorption peaks of copolymer microsphere n-PSTb-4 have a red shift (Figure S12, Supporting Information), which indicates that the coordination structure of Tb-complex in copolymer microspheres has changed. The change of coordination structure further affects the efficiency of ligand-to-Tb energy transfer, and eventually leads to the fluorescence quenching of the copolymer microspheres.[46] Additionally, the absorption spectra of the Tb-complex monomer $Tb(AA)_3Phen$ after mixing with Fe^{3+} showed a red shift similarly as that of copolymer microsphere n-PSTb-4 (Figure S13, Supporting Information); and the fluorescence of $Tb(AA)_3Phen$ was also completely quenched with addition of Fe^{3+} (Figure S14, Supporting Information). These results further demonstrate that the fluorescence quenching of copolymer microspheres is due to the change of coordination structure result from the interaction of Tb-complexes with Fe^{3+} in copolymer microspheres.

The porosity of the copolymer microspheres is more beneficial to the interaction of iron ions with the Tb-complexes. Therefore, with the increase of the Tb-complex content (<2.5 wt%), K_{SV} increased, and LOD gradually decreased (Table 2). In comparison with n-PSTb-4, the fluorescence intensity of n-PSTb-5 increased; but the BET surface area of n-PSTb-5 decreased slightly; consequently, K_{SV} of n-PSCz-5 decreased and LOD increased slightly. Briefly, intense fluorescence and large BET surface area endow the copolymer microspheres with wide detection range and low detection limit for Fe^{3+} in aqueous environment.

4. Conclusions

Novel covalently bonded Tb-complex-containing copolymer microspheres were successfully prepared through a simple one-step soap-free emulsion polymerization. The obtained copolymer microspheres exhibit a stable spherical morphology with a narrow size distribution, excellent thermal stability, probably BET surface area, and intense and stable green luminescence. Particularly, the limit of detection (LOD) of the copolymer microspheres for Fe^{3+} in aqueous medium could be as low as 2.1 μM, and the tolerance level of detection of Fe^{3+} can be as high as 1500 μM. The fluorescence quenching of the copolymer microspheres may be attributed to the interaction of iron ions with nitrogen and oxygen atoms of ligands, which changes the coordination structure of Tb-complexes, thereby affecting the energy transfer from ligands to Tb^{3+}. Our study provides useful references for the future design of covalently-bonded lanthanide-based copolymer microspheres sensors targeting for biological detection and environmental challenges.

Supporting Information

Supporting Information is available from the Wiley Online Library or from the author.

Acknowledgements

This work was financially supported by the National Natural Science Foundation of China (Nos. 21802039, 21674129), the Scientific Research Fund of Hunan Provincial Education Department (No. 16B064), the National Students' project for innovation and entrepreneurship training program (No. 201811528001), Hunan province college students' research learning and innovative experiment project, Key Laboratory of green functional building materials of Hunan Institute of Technology and the construct program of the key discipline in Hunan province.

Conflict of Interest

The authors declare no conflict of interest.

Keywords

fluorescence sensors, iron ions, luminescence, polymer microspheres, Tb-complex

Received: September 5, 2018
Revised: November 1, 2018
Published online: November 23, 2018

[1] R. Das, C. D. Vecitis, A. Schulze, B. Cao, A. F. Ismail, X. B. Lu, J. P. Chen, S. Ramakrishna, *Chem. Soc. Rev.* **2017**, *46*, 6946.
[2] H. Zhu, J. L. Fan, B. H. Wang, X. J. Peng, *Chem. Soc. Rev.* **2015**, *44*, 4337.

[3] S. K. Sahoo, D. Sharma, R. K. Bera, G. Crisponi, J. F. Callan, *Chem. Soc. Rev.* **2012**, *41*, 7195.
[4] H. Sharma, N. Kaur, A. Singh, A. Kuwar, N. Singh, *J. Mater. Chem. C* **2016**, *4*, 5154.
[5] H. Q. Zhang, Y. H. Huang, X. H. Lin, F. F. Lu, Z. S. Zhang, Z. B. Hu, *Sens. Actuators, B* **2018**, *255*, 2218.
[6] L. Z. Zhang, Q. Li, J. P. Zhou, L. N. Zhang, *Macromol. Chem. Phys.* **2012**, *213*, 1612.
[7] Q. Zhang, B. Wu, D. Zhong, X. W. Zhan, G. J. Wang, *Macromol. Rapid Commun.* **2016**, *37*, 2052
[8] Y. Zhan, Y. L. Liu, Q. Q. Liu, Z. M. Liu, H. Y. Yang, B. F. Lei, J. L. Zhuang, C. F. Hu, *Sens. Actuators, B* **2018**, *255*, 290.
[9] R. Atchudana, T. N. J. I. Edison, K. R. Aseer, S. Perumal, N. Karthik, Y. R. Lee, *Biosens. Bioelectron.* **2018**, *99*, 303.
[10] N. K. Das, S. Ghosh, A. Priya, S. Datta, S. Mukherjee, *J. Phys. Chem. C* **2015**, *119*, 24657.
[11] C. H. Lu, J. Cao, Y. X. Cheng, Y. H. Jin, Y. Qu, J. L. Xu, *Sens. Actuators, B* **2018**, *255*, 3102.
[12] S. Dang, T. Wang, F. Y. Yi, Q. H. Liu, W. T. Yang, Z. M. Sun, *Chem. Asian J.* **2015**, *10*, 1703.
[13] M. Schäferling, *Angew. Chem. Int. Ed.* **2012**, *51*, 3532.
[14] L. M. Zhang, B. Li, Z. M. Su, S. M. Yue, *Sens. Actuators, B* **2010**, *143*, 595.
[15] X. Shen, B. Yan, *RSC Adv.* **2015**, *5*, 6752.
[16] K. Ghosh, E. R. M. Balog, J. L. Kahn, D. P. Shepherd, J. S. Martinez, R. C. Rocha, *Macromol. Chem. Phys.* **2015**, *216*, 1856.
[17] H. E. Zhu, J. Tao, W. H. Wang, Y. J. Zhou, P. H. Li, Z. Li, K. Yan, S. L. Wu, K. W. K. Yeung, Z. S. Xu, H. B. Xu, P. K. Chu, *Biomaterials* **2013**, *34*, 2296.
[18] A. I. Abdelrahman, S. Dai, S. C. Thickett, O. Ornatsky, D. Bandura, V. Baranov, M. A. Winnik, *J. Am. Chem. Soc.* **2009**, *131*, 15276.
[19] Y. Liang, A. I. Abdelrahman, V. Baranov, M. A. Winnik, *Polymer* **2011**, *52*, 5040.
[20] J. B. Tan, G. Y. Zhao, Z. H. Zeng, M. A. Winnik, *Macromolecules* **2015**, *48*, 3629.
[21] S. Zhang, B. Ma, S. C. Wang, J. Z. Duan, J. C. Qiu, D. Li, Y. H. Sang, S. H. Ge, H. Liu, *Chem. Eng. J.* **2018**, *331*, 675.
[22] B. Chen, G. A. Wen, J. J. Wu, J. C. Feng, *Macromol. Rapid Commun.* **2015**, *36*, 1836.
[23] J. F. Li, F. Li, X. X. Jiang, G. Wei, Y. X. Cheng, C. J. Zhu, *Macromol. Rapid Commun.* **2013**, *34*, 1312.
[24] B. J. Gao, L. Fang, J. Y. Men, *Polymer* **2012**, *53*, 4709.
[25] J. X. Luo, C. Y. Zhang, C. H. Li, H. X. Hua, B. N. Hu, *RSC Adv.* **2014**, *4*, 57393.
[26] C. J. Xu, B. G. Li, *Macromol. Chem. Phys.* **2010**, *211*, 1733.
[27] Z. J. Li, H. W. Zhang, J. S. Shen, *Polym. Compos.* **2011**, *32*, 1712.
[28] L. J. Wang, X. Wang, T. X. Wang, Z. J. Hu, G. Zou, Q. J. Zhang, *J. Mater. Sci.* **2012**, *47*, 2600.
[29] L. Guo, B. Yan, *Photochem. Photobiol.* **2010**, *86*, 1185.
[30] B. Yan, M. Guo, *J. Photochem. Photobiol., A.* **2013**, *257*, 34.
[31] P. Fabbri, S. Mohammad Poor, L. Ferrari, L. Rovati, L. D. Carlos, *Polymer* **2014**, *55*, 488.
[32] C. X. Liu, T. R. Wang, D. Q. Yang, Z. Q. Li, H. R. Li, *Chem. - Asian J.* **2017**, *12*, 768.
[33] S. Ali, Z. Zuhra, I. S. Butler, S. U. Dar, M. U. Hameed, D. Z. Wu, L. Q. Zhang, Z. P. Wu, *Chem. Eng. J.* **2017**, *315*, 448.
[34] J. X. Luo, C. L. Yang, J. Zheng, J. Y. Ma, L. Y. Liang, M. G. Lu, *Eur. Polym. J.* **2011**, *47*, 385.
[35] H. M. Ni, Y. Z. Du, G. H. Ma, M. Nagai, S. Omi, *Macromolecules* **2001**, *34*, 6577.
[36] F. Wen, W. Q. Zhang, P. W. Zheng, X. Zhang, X. L. Yang, Y. Wang, X. W. Jiang, G. W. Wei, L. Q. Shi, *J. Polym. Sci., Part A: Polym. Chem.* **2008**, *46*, 1192.
[37] S. F. Wu, Y. Liu, G. P. Yu, J. G. Guan, C. Y. Pan, Y. Du, X. Xiong, Z. G. Wang, *Macromolecules* **2014**, *47*, 2875.
[38] S. Kandambeth, A. Mallick, B. Lukose, M. V. Mane, T. Heine, R. Banerjee, *J. Am. Chem. Soc.* **2012**, *134*, 19524.
[39] Q. Chen, D. P. Liu, M. Luo, L. J. Feng, Y. C. Zhao, B. H. Han, *Small* **2014**, *10*, 308.
[40] Y. Zhou, H. H. Chen, B. Yan, *J. Mater. Chem. A* **2014**, *2*, 13691.
[41] B. Bonillo, R. S. Sprick, A. I. Cooper, *Chem. Mater.* **2016**, *28*, 3469.
[42] A. Baral, K. Basu, S. Roy, A. Banerjee, *ACS Sustainable Chem. Eng.* **2017**, *5*, 1628.
[43] Z. H. Xiang, C. Q. Fang, S. H. Leng, D. P. Cao, *J. Mater. Chem. A* **2014**, *2*, 7662.
[44] Y. Song, R. Q. Fan, X. Du, K. Xing, Y. W. Dong, P. Wang, Y. L. Yang, *RSC Adv.* **2016**, *6*, 110182.
[45] R. Li, X. L. Qu, Y. H. Zhang, H. L. Han, X. Li, *CrystEngComm.* **2016**, *18*, 5890.
[46] X. Y. Dong, R. Wang, J. Z. Wang, S. Q. Zang, T. C. W. Mak, *J. Mater. Chem. A* **2015**, *3*, 641.